Desalination and Water Treatment
www.deswater.com

doi: 10.1080/19443994.2016.1152641

57 (2016) 24626–24635
November

Taylor & Francis
Taylor & Francis Group

Jet quality characteristics according to nozzle shape of energy-recovery Pelton turbines in pressure-retarded osmosis

In Chan Jo[a,b], Joo Hoon Park[a,b], Jeong-Won Kim[a], Youhwan Shin[b,*], Jin Taek Chung[c]

[a]*Graduate School of Korea University, Innovation Hall 332, Korea University, Anam-ro 145, Seongbuk-gu, Seoul 136-713, Korea, emails: jic7139@korea.ac.kr (I.C. Jo), joohoon82@korea.ac.kr (J.H. Park), jwkim@korea.ac.kr (J.-W. Kim)*

[b]*Center for Urban Energy Research, Korea Institute of Science and Technology, Hwarangno 14-gil 5, Seongbuk-gu, Seoul 136-791, Korea, email: yhshin@kist.re.kr*

[c]*Department of Mechanical Engineering, Korea University, Innovation Hall 310, Anam-ro 145, Seongbuk-gu, Seoul 136-713, Korea, email: jchung@korea.ac.kr*

Received 23 October 2015; Accepted 8 January 2016

ABSTRACT

Pelton turbines are used for energy recovery in pressure-retarded osmosis (PRO) systems. The quality of jet sprays is a significant factor affecting the performance of these turbines. This study examined jet quality characteristics according to the nozzle geometry of Pelton turbines. Jet quality tests were conducted to analyze the degree of similarity between the actual jet flow and the ideal jet flow. Power loss, discharge coefficients, and performance characteristics of Pelton turbines were examined with respect to the nozzle shape through performance tests of the nozzles and turbines. Furthermore, jet flows were numerically analyzed. The test results and analyses confirm that for a given input power, the recirculation region increases and the jet quality decreases with increasing nozzle throat angle. On the basis of the results, the optimum range of nozzle throat angle for Pelton turbines in PRO systems is suggested.

Keywords: Energy recovery Pelton turbine; Jet quality; Nozzle throat angle; Nozzle coefficient; Pressure-retarded osmosis

1. Introduction

With rapid population growth and industrialization, global air pollution and water scarcity have become serious considerations. In response, nations worldwide have focused on developing technologies to harvest various alternative energy resources, such as solar, hydro, marine, and wind energy. In particular, power technologies using salinity gradients of sea water and fresh water have received much attention. Among the various alternative power generation technologies under development for energy recovery based on salinity difference, pressure-retarded osmosis (PRO) is being actively researched [1–3]. PRO, a term coined by Loeb in 1976 in a great contribution to PRO system studies [4,5], is a power generation method based on osmotic energy. In this method, a feed

*Corresponding author.

Presented at 2015 Academic Workshop for Desalination Technology held in the Institute for Far Eastern Studies Seoul, Korea, 23 October 2015

solution passes through a semipermeable membrane by osmosis to become a draw solution with higher hydraulic pressure. This hydraulic pressure is converted to electrical energy through the use of an energy-recovery device (ERD). PRO theory has been actively studied and improved by Thorsen and Holt, and Statkraft Co., constructed a prototype PRO plant in 2009 [6,7]. In 2010, RO/PRO composite processes were studied in the megaton projects in Japan. Fig. 1 illustrates a schematic of a PRO system.

The Pelton turbine is suitable as the ERD in PRO systems because it operates at high pressure and low flow volumes. It is a representative impulse-type hydraulic turbine, in which jet sprays from a nozzle impact a bucket to create an axis rotation, thereby generating power. The jet pressure energy is converted to kinetic energy by a runner, which is then converted to electrical energy by a generator. An energy-recovery Pelton turbine is composed simply of a nozzle, bucket, runner, and generator. Among various factors that affect the efficiency of Pelton turbines (operating conditions, bucket and runner geometry, bucket size, and jet quality), the quality of jet sprays has a significant effect.

In previous studies on jet quality, Peron et al. [8] analyzed Pelton turbine noise using computational fluid dynamics (CFD) analysis and jet visualization and improved the efficiency of the turbines by redesigning them to reduce the formation of vortices in the injector, which improved the jet quality. Zhang and Casey [9] conducted laser Doppler anemometry to determine how the secondary flows inside jets (created by bends and bifurcations) affect the jet quality. Furthermore, Tesar [10] studied the separation layer thickness of reduced parts according to shape variations inside a simple nozzle, and Tuan et al. [11] experimentally confirmed that flow rates and pressure conditions of jet sprays change according to shape variations inside such a nozzle. Previous studies described ideal jets as jets that spray over a constant area along the vertical or horizontal axis in the direction of jet flow [8]. Jet quality reflects the degree of similarity between an actual jet flow and an ideal jet flow. Jet quality is higher if the flow spread is smaller and the separation layer is thinner around the narrow part inside the nozzle, thus reducing flow loss [12,13]. However, because of nozzle characteristics such as geometry and roughness, jets have complex flow structures in actual applications. According to a previous study [9], as the separation region increases, energy loss—an important element of jet quality—increases as well. In this study, a test was conducted to compare the performance characteristics of Pelton turbines and nozzles according to throat angle, and a CFD analysis was performed to determine the characteristics of nozzle interiors and jet flows to evaluate jet quality.

2. Performance test

To simulate the operating conditions of a high-pressure concentrate generated from membranes in a

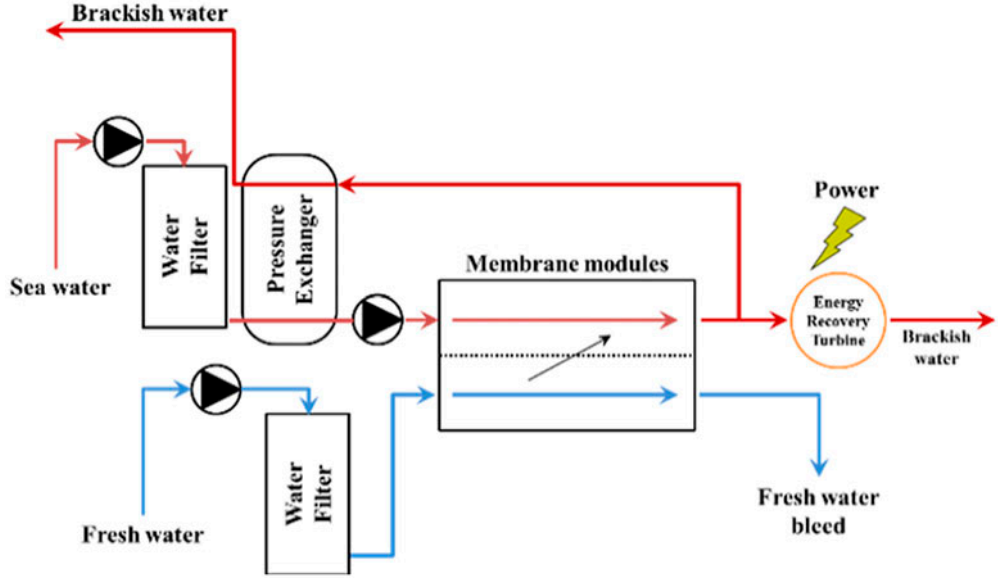

Fig. 1. Schematic of PRO.

PRO system, high-pressure piston-type pumps were used (Fig. 2). To measure the nozzle pressure, a pressure transducer was installed and a turbine-type flow meter was used. The turbine and a servo motor were connected directly to measure torque using a torque transducer around the axis, and rotational velocities were controlled using the servo motor. To examine jet quality with varying nozzle throat angles, five nozzles with different throat angles (30˚, 60˚, 85˚, 120˚, and 180˚) were manufactured (Fig. 3). Nineteen Pelton turbine buckets were manufactured using 3D printing technology for convenience. The performance test was conducted by varying the rotational speed with the servo motor. The flow rate, pressure, shaft torque, and rotational speeds were measured, and nozzle and turbine performance was analyzed.

In the jet quality analyses, changes in the nozzle discharge coefficient according to the throat angle were investigated. The mass ratio of the theoretical jet flow to the actual flow at the nozzle outlet is referred to as the discharge coefficient (Eq. (1)). This value gages the nozzle's efficiency and is closely related to jet quality. A greater value results in a higher degree of similarity between the actual flow and the theoretical flow [14,15].

$$C_D = \frac{4 \cdot \dot{m}}{\pi \cdot D^2 \cdot \sqrt{2 \cdot \rho \cdot P}} \quad (1)$$

The velocity coefficient in Eq. (2) represents the ratio of actual velocity to theoretical velocity of the jet flow

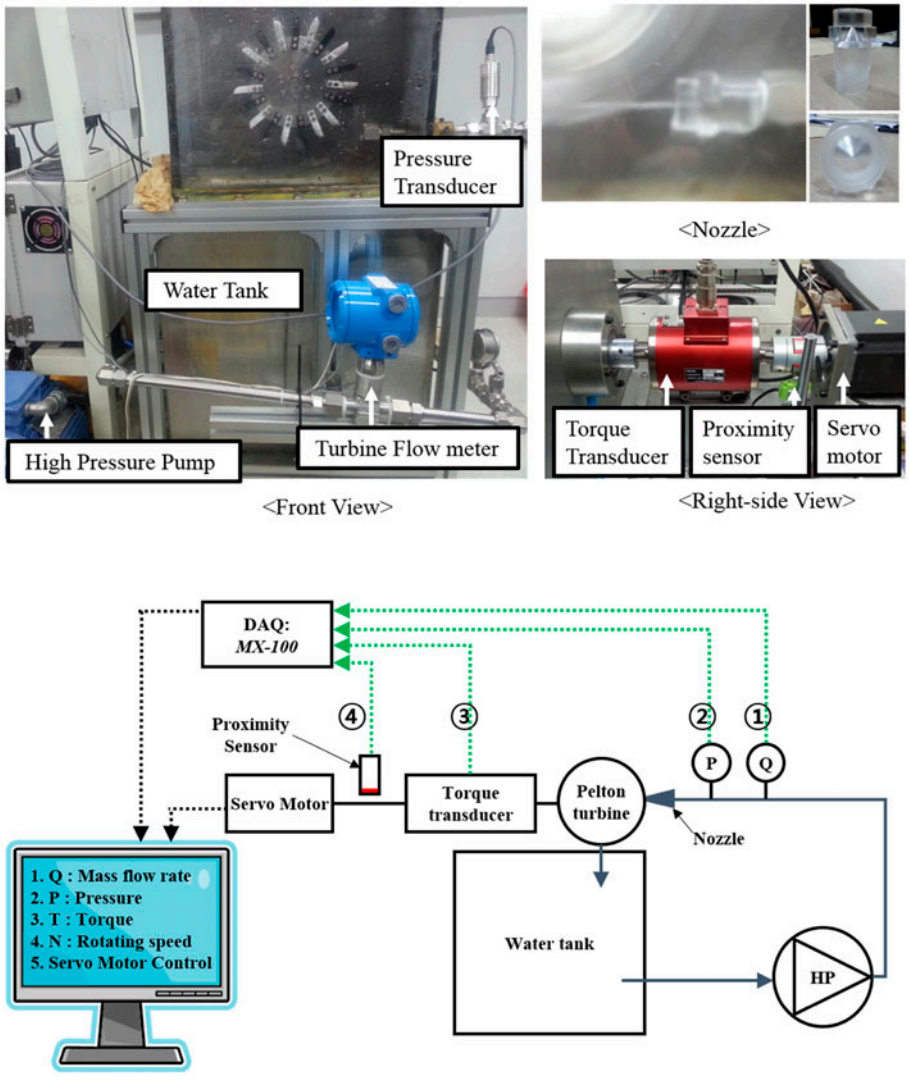

Fig. 2. Pelton turbine performance test apparatus (top) and its schematic.

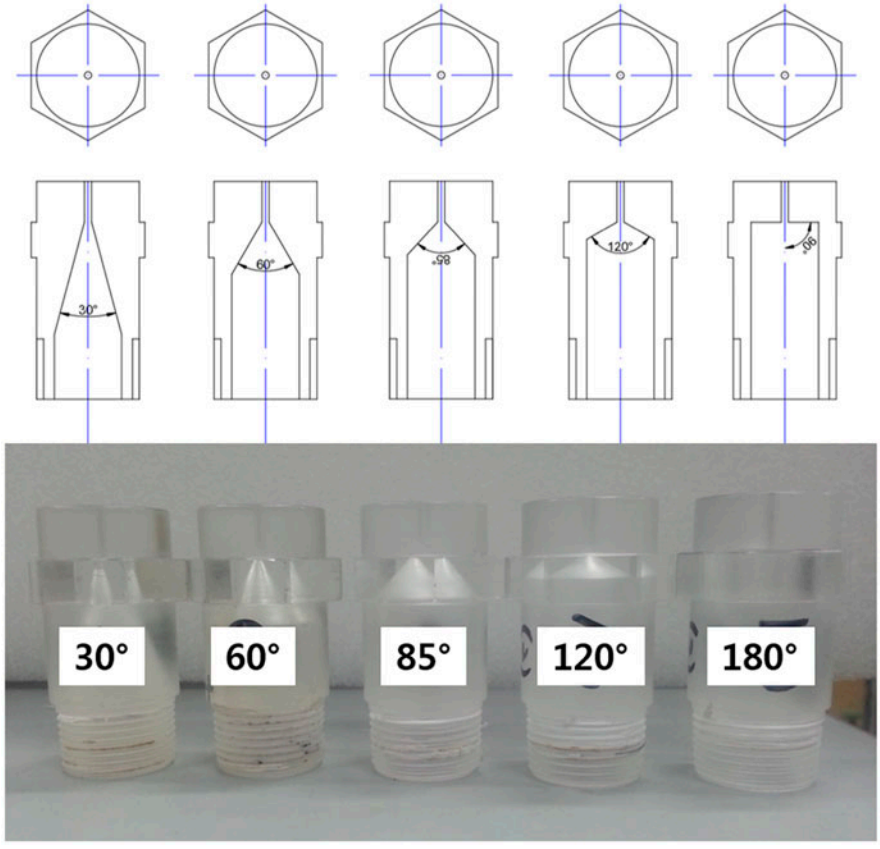

Fig. 3. Nozzle drawings (top) and photographs.

from the nozzle. These values are always below one because of friction loss, and therefore, can be used to indicate the degree of friction loss within the nozzle.

$$C_V = \frac{V_{jet}}{\sqrt{2 \cdot P/\rho}} \tag{2}$$

The power at a given location can be calculated using Eq. (3). The percentage of power loss, as expressed in Eq. (4), is power loss in the nozzle divided by the input power generated when the fluid passes through the throat inside the nozzle. The power loss is calculated as the loss across the location where the nozzle starts to narrow (Location 1) and the nozzle's outlet (Location 2). Because the difference in potential energy between these two locations can be considered negligible, the corresponding term is removed in Eq. (3). Moreover, because atmospheric pressure is considered at Location 2, only velocities are included in the calculation.

$$\text{Power at a location } [W] = \dot{m}\left(\frac{P}{\rho} + \frac{v^2}{2} + gz\right) = P \cdot Q + \frac{\dot{m} \cdot v^2}{2} \tag{3}$$

$$\left(v = \frac{Q}{A}\right)$$

$$\text{Percentage of power loss } (\%) = \frac{\text{Energy loss}}{\text{Input energy}} = \frac{\Delta\text{Energy}_{\text{Location1}\rightarrow 2}}{\text{Energy}_{\text{Location1}}} \tag{4}$$

3. Numerical analysis methods

3.1. Nozzle configuration

Fig. 4 illustrates the nozzle geometry for CFD analysis, where A is the throat angle. The length of the nozzle's throat (D) (11.5 mm) as well as total length of

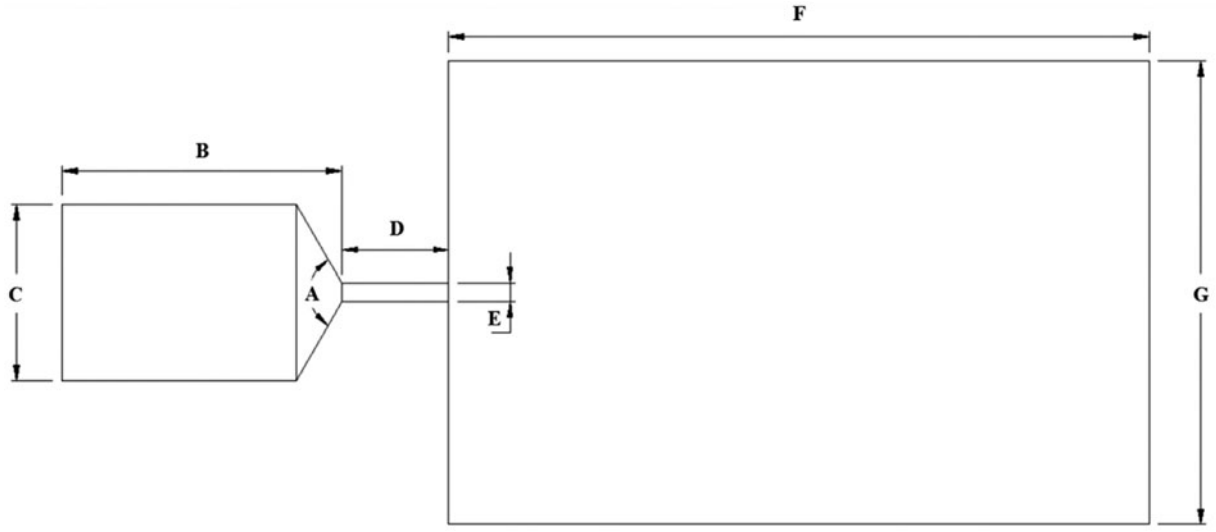

Fig. 4. Nozzle geometry for CFD analysis with fixed and variable geometric parameters.

the nozzle (B + D) were set constant. The nozzle's inlet diameter (C) was 19 mm, identical to that of the pipes used in the experiment apparatus. And section (E) is the nozzle's outlet. In the simulation, the jet sprayed from the nozzle hits the Pelton turbine's bucket, and the distance of the jet was measured as the distance from the nozzle outlet to the bucket (F). The length (G) at which the jet mixed with air and dispersed by air friction was determined to be 35 times the nozzle outlet diameter.

3.2. Analysis settings

The boundary conditions for the CFD analysis are given in Table 1. ANSYS CFX 14.5 was used for the analysis. Because jet flow is a mixture of water and air, a homogeneous model was used for the multiphase method, and gravity conditions were set. For multiphase free-surface simulation, a k–ω SST turbulence model and a high-resolution advection scheme were applied. A residual target of 1×10^{-5} or less was used for the solver convergence criteria, and the imbalance values of mass, pressure, and momentum were determined to be 1% or less.

3.3. Mesh

Because the jet flow of a rapidly narrowing nozzle throat is complex, the Y^+ value for the first mesh near the wall was set to two or lower. A hexahedral mesh was generated using ANSYS ICEM CFD 14.5, and the mesh quality was enhanced using an O-grid at the round part. The mesh was verified by proportionally increasing the number of nodes on the X-, Y-, and Z-axes, and the calculated nozzle inlet static pressures were compared according to the number nodes (Fig. 5). It was confirmed that for a constant number of nodes, the inlet static pressure values converge. The number of nodes finally selected was 5.7 million.

4. Results and discussion

4.1. Test results

Fig. 6 shows a hill chart comparing the input power of the nozzles according to flow rate and pressure. The nozzle input pressures were measured by increasing the fluid volume for each nozzle (30°, 60°, 85°, 120°, and 180°). The input power increases as both flow volume and pressure increase simultaneously

Table 1
Boundary conditions for numerical analysis

Location	Boundary	Boundary details
Nozzle inlet	Inlet	Mass and momentum: Bulk mass flow rate
Nozzle surface	Wall	Mass and momentum: No slip wall Wall roughness: Smooth wall
Nozzle outlet and chamber region	Opening	Mass and momentum: Opening (atmospheric pressure) Acceleration of gravity (9.806 m/s^2)

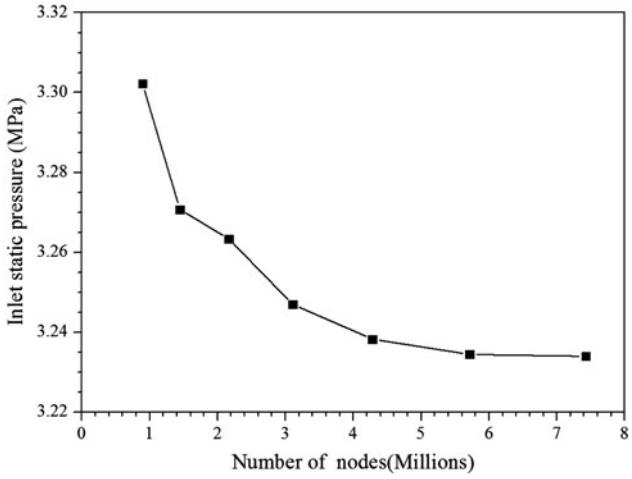

Fig. 5. Results of mesh independence.

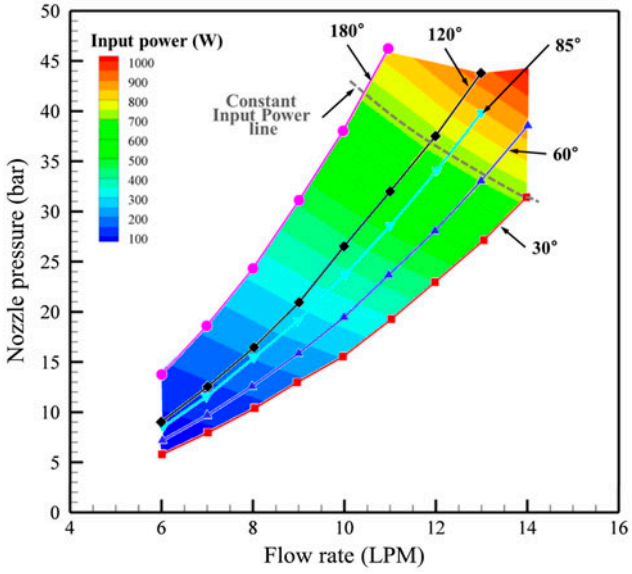

Fig. 6. Pump operating characteristics for different nozzle throat angles.

according to the pump's operating characteristics. As the nozzle throat angle increases, the ratio of pressure increase with increasing flow rate gradually rises. Furthermore, for a given flow rate, the pressure inside the nozzle increases as the nozzle throat angle increases. Under a given pressure, however, the flow rate decreases with increasing nozzle throat angle, likely because the flow section area decreases because of recirculation generated in the throat as the angle inside the nozzle increases. (This is later explained through the results of CFD analysis of the flow inside the nozzle.) The performance tests on the nozzles and Pelton turbines were conducted at constant input power (gray dashed line in Fig. 6).

Under a given input power, as the nozzle throat angle increases, the turbine's maximum efficiency decreases (Fig. 7). This is likely because jet spray power decreases as the nozzle throat angle increases, thus reducing the turbine's shaft power. Therefore, a higher nozzle throat angle results in a greater loss of power as well as larger reduction in jet quality.

The performance test showed no significant change in the flow rate for both discharge and velocity coefficients. However, both these coefficients decrease as the nozzle throat angle increases (Fig. 8). The decreasing trend of discharge coefficient is a result of increasing deviation of the characteristics of actual flow from those of the ideal flow as the throat angle increases. The trend of velocity coefficient changes is a result of gradual increase in the friction loss as the nozzle throat angle increases.

Fig. 9 shows the results of power loss calculations. The percentage of power loss is not affected by flow rate variations and increases with increasing nozzle throat angle.

4.2. Numerical analysis results

Fig. 10 illustrates changes in static pressure along the fluid path for various nozzle throat angles. Streamwise locations range from a point approximately 10 mm from the nozzle throat to a part of the jet area outside the nozzle outlet. The static pressure at each nozzle inlet corresponds to the pressure of constant input power explained in Fig. 6. Before the flow reaches the nozzle throat, the pressure changes in pro-

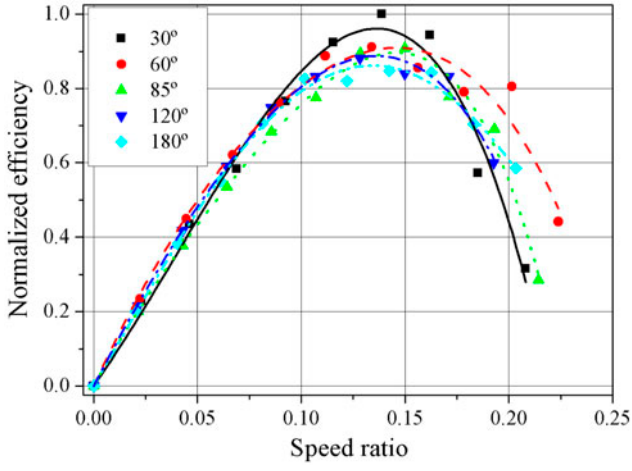

Fig. 7. Speed ratio vs. Pelton turbine efficiency for different nozzle throat angles.

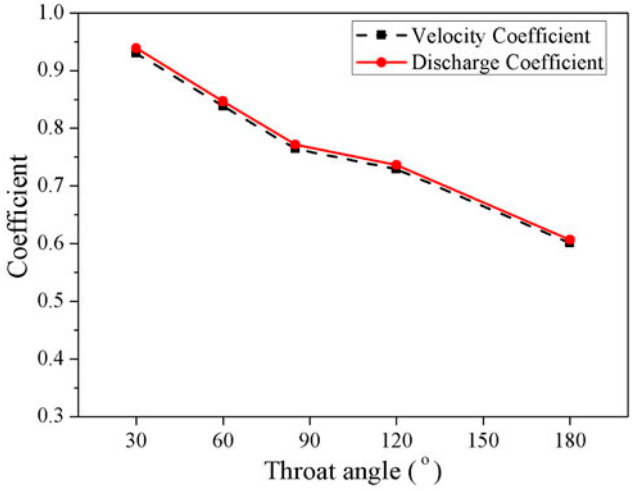

Fig. 8. Throat angle vs. velocity coefficient and discharge coefficient.

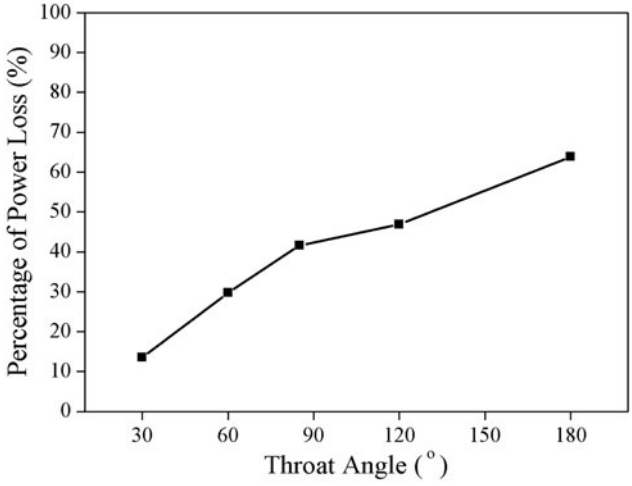

Fig. 9. Throat angle vs. percentage of power loss.

portion to the increment of the angle. This is likely because the length of the flow path inside the nozzle decreases as the throat angle increases, rapidly changing the slope of static pressure in Fig. 10. The static pressure changes between the nozzle throat and the nozzle outlet are very similar at 30˚ and 60˚. However, for 85˚ and greater values, a static pressure overshoot occurs, the degree of which increases with the angle. This is likely because a recirculation region is formed by the separation at the edge of the nozzle throat, and as the throat angle increases, the size of the recirculation region also increases. This recirculation region reduces the sectional area of the nozzle throat, thus

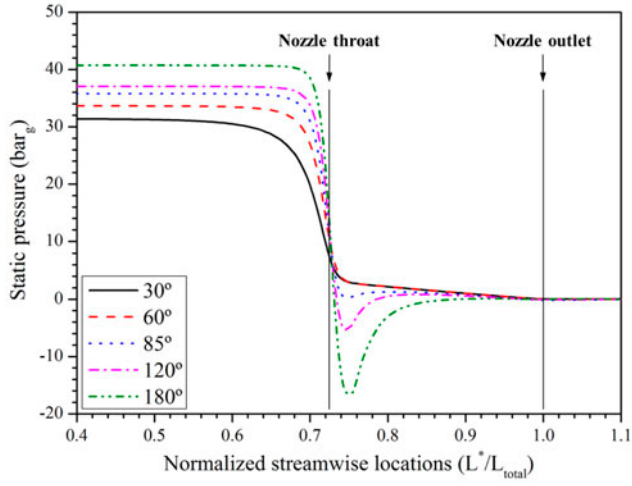

Fig. 10. Change in static pressure along the flow path inside the nozzle for different nozzle throat angles.

rapidly increasing the local flow velocity, which creates a rapid pressure reduction.

Velocity changes in the narrowed area inside the nozzle were investigated for each throat angle. Fig. 11 illustrates the velocity contours in areas surrounding the nozzle throat (for qualitative evaluation) for throat angles of 30˚, 85˚, and 180˚. A local velocity increase at the nozzle throat and a recirculation region form symmetrically along the axis. The white dotted lines in Fig. 11(b) and (c) represent the separation streamlines with points of zero velocity in the recirculation region. Fig. 11 confirms that the size of the recirculation region increases with increasing throat angle. Because of rapid changes in the flow direction and in the sectional area at the throat, a recirculation region forms; this region grows as the throat angle inside the nozzle increases, because the degree of changes becomes more abrupt. Table 2 lists the recirculation region's maximum thickness values for different throat angles obtained from the numerical analysis. The values explain how the ratio of pressure rise increases with the nozzle throat angle (Fig. 6) according to an increase in flow rate.

The relationship between the pressure head H, flow rate Q, and discharge coefficient C_D is expressed in Eqs. (5) and (6). The value on the left-hand side of Eq. (6) represents the slope in Fig. 6; it increases as the flow rate increases under a constant throat angle (A). Furthermore, as the nozzle throat angle increases, its recirculation region also increases, reducing the cross-sectional area of the jet flow passing through the nozzle. This explains the increase in the slope with increasing throat angle under a constant flow rate.

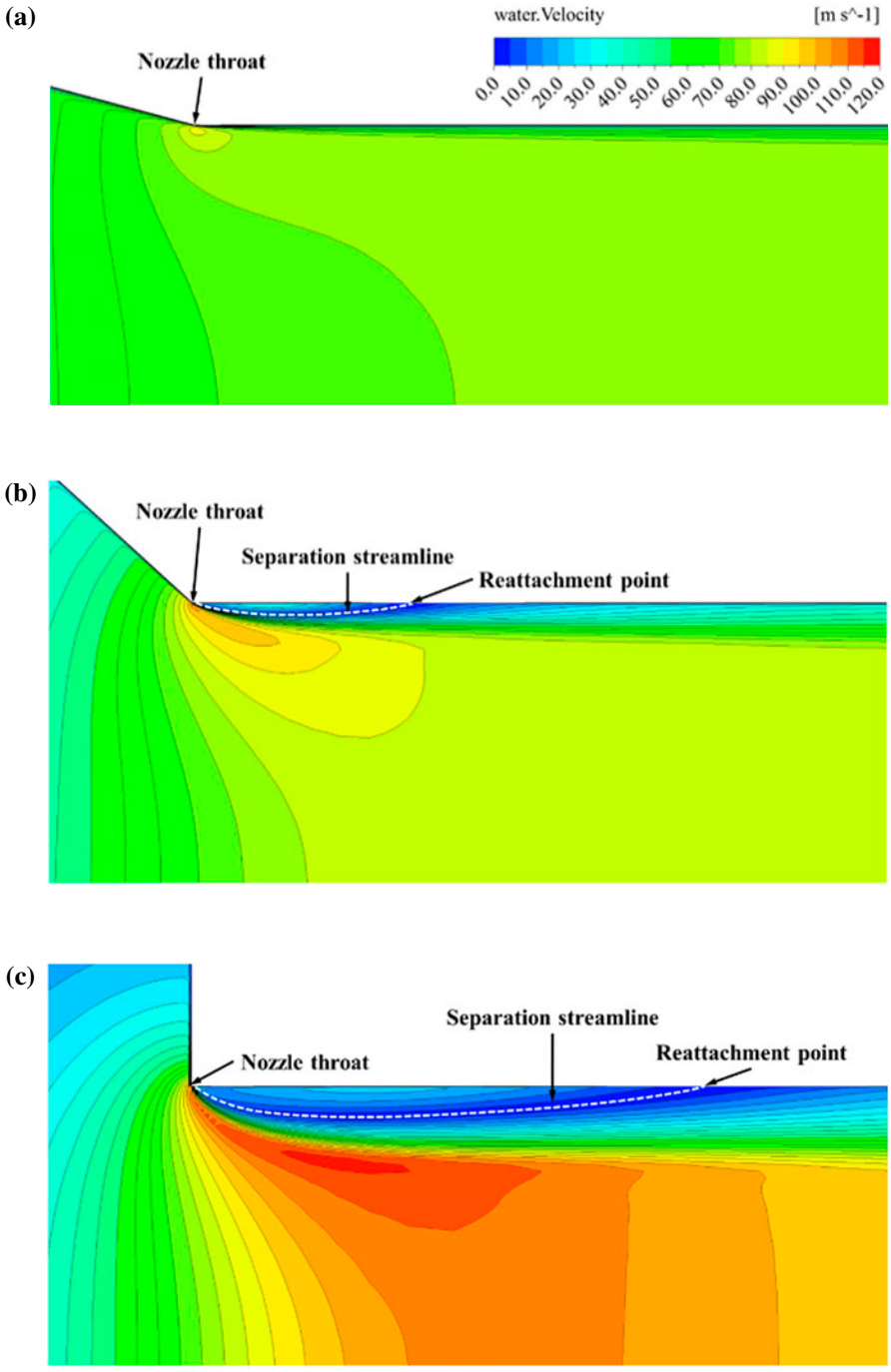

Fig. 11. Velocity contours of nozzle throat at inner angles of nozzle: (a) throat angle 30˚, (b) throat angle 85˚, and (c) throat angle 180˚.

$$A_{\text{nozzle}} = \frac{4 \cdot Q}{\pi \cdot C_{\text{d}} \sqrt{2g}} \cdot \frac{1}{H^{1/2}} \tag{5}$$

$$\frac{\mathrm{d}H}{\mathrm{d}Q} \propto 2\frac{Q}{A^2} \tag{6}$$

Fig. 12 presents the numerical analysis results of the axial jet velocity distribution at certain points (0D, 1D, 5D, 10D, and 20D) along the flow path between the nozzle outlet and the Pelton bucket. The normalized jet velocity at areas below the jet is smaller because of gravity, and the velocity curves become more irregular

Table 2
Maximum separation layer thickness for each throat angle

Throat angle of nozzle (˚)	Maximum separation layer thickness (mm)
30	0
60	0.010
85	0.030
120	0.047
180	0.100

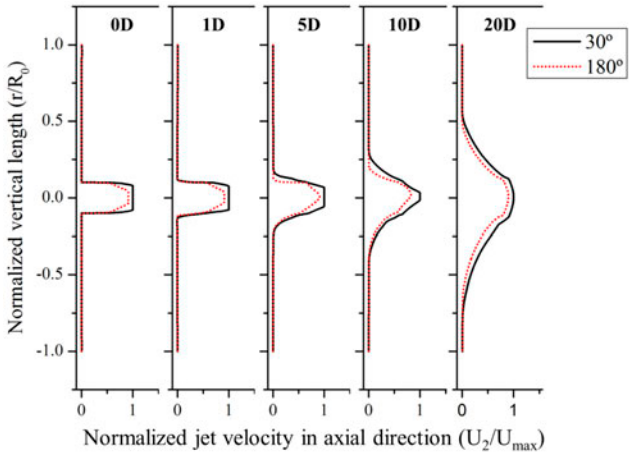

Fig. 12. Normalized jet velocity in the axial direction at specific distances between the nozzle outlet and Pelton bucket.

as the jet spray moves farther from the nozzle outlet because of continual air friction within the casing. The degree of irregularity is aggravated by increasing nozzle throat angle, indicating a decrease in the jet quality. As a result, a throat angle of 180˚ yields a lower turbine efficiency than the efficiency of 30˚, as shown in Fig. 7.

5. Conclusion

In this study, a performance test was conducted on an energy-recovery turbine according to changes in the throat angle of the nozzle, and it was confirmed through a numerical analysis that the size of separation region changes in certain areas of the nozzle throat. The following conclusions can be drawn from the results:

(1) In general, as the nozzle throat angle increases, jet velocity becomes nonuniform and flow power decreases, which affects the Pelton turbine efficiency. Under a given input power flow into the nozzle, as the throat angle increases, the turbine efficiency decreases.
(2) Analysis of the nozzle discharge coefficients confirmed that, as the throat angle increases, the actual flow becomes more dissimilar from the ideal flow in certain aspects and friction loss in the nozzle gradually increases.
(3) As the throat angle increases, the recirculation region is generated at the end of the throat region also increases, reducing the cross-sectional area of the flow passing through the nozzle and thus increasing power loss.

Overall, higher nozzle throat angles result in lower turbine efficiency, discharge coefficient, and velocity coefficient and greater power loss, all of which contribute to reduced jet quality. Therefore, the optimum nozzle throat angle of energy-recovery turbines in PRO systems is 30˚ or less.

Acknowledgment

This research was supported by a grant (code 13IFIP-B065893-03) from Industrial Facilities & Infrastructure Research Program funded by Ministry of Land, Infrastructure and Transport of Korean government.

References

[1] F. Helfer, C. Lemckert, Y.G. Anissimov, Osmotic power with pressure retarded osmosis: Theory, performance and trends—A review, J. Membr. Sci. 453 (2014) 337–358.
[2] A. Achilli, T.Y. Cath, A.E. Childress, Power generation with pressure retarded osmosis: An experimental and theoretical investigation, J. Membr. Sci. 343 (2009) 42–52.
[3] I.L. Alsvik, M.B. Hägg, Pressure retarded osmosis and forward osmosis membranes: Materials and methods, Polymers 5 (2013) 303–327.
[4] S. Loeb, Production of energy from concentrated brines by pressure-retarded osmosis: I. Preliminary technical and economic correlations, J. Membr. Sci. 1 (1976) 49–63.

[5] S. Loeb, F. Van Hessen, D. Shahaf, Production of energy from concentrated brines by pressure-retarded osmosis: II. Experimental results and projected energy costs, J. Membr. Sci. 1 (1976) 249–269.
[6] Statkraft Home Page. Available from: <http://www.statkraft.com/> (accessed 15 December 2015).
[7] S.E. Skilhagen, J.E. Dugstad, R.J. Aaberg, Osmotic power—Power production based on the osmotic pressure difference between waters with varying salt gradients, Desalination 220 (2008) 476–482.
[8] M. Peron, E. Parkinson, L. Geppert, T. Staubli, Importance of jet quality on Pelton efficiency and cavitation, in: IGHEM 2008, September, Milan, Italy, 2008, pp. 1–9.
[9] Z. Zhang, M. Casey, Experimental studies of the jet of a Pelton turbine, Proc. Inst. Mech. Eng. Part A J. Power Energy 221 (2007) 1181–1192.
[10] V. Tesař, Characterisation of inexpensive, simply-shaped nozzles, Chem. Eng. Res. Des. 88 (2010) 1433–1444.
[11] T.N. Tuan, H. Okada, T. Tsukamoto, K. Ohe, K. Iwasawa, Effect of rounding-off nozzle hole inlet on fuel injection and combustion characteristics under high-temperature and high-pressure, J. Jpn. Inst. Mar. Eng. 42 (2007) 288–294 (translated).
[12] Z. Zhang, Inlet flow conditions and the jet impact work in a Pelton turbine, Proc. Inst. Mech. Eng. Part A J. Power Energy 223 (2009) 589–596.
[13] Z. Zhang, E. Parkinson, LDA application and the dual-measurement-method in experimental investigations of the free surface jet at a model nozzle of a Pelton turbine, in: Proceedings of the 11th International Symposium on Applications of Laser Anemometry to Fluid Mechanics, Lisbon, Portugal, 2002.
[14] E. Ghassemieh, H.K. Versteeg, M. Acar, The effect of nozzle geometry on the flow characteristics of small water jets, Proc. Inst. Mech. Eng. Part C J. Mech. Eng. Sci. 220 (2006) 1739–1753.
[15] J.M. Desantes, R. Payri, F.J. Salvador, J. Gimeno, Measurements of spray momentum for the study of cavitation in diesel injection nozzles, SAE Technical Paper 2003-01-0703 (2003).